

## Article

# A Coordination Polymer Based on Nickel(II)–Cyamelurate: A Robust Catalyst with Highly Dispersed Nickel Sites for Nitrophenol Reduction under Ambient Conditions

Taís dos Santos da Cruz<sup>1</sup>, Walker Vinícius Ferreira do Carmo Batista<sup>1</sup>, Eduarda Ferreira de Oliveira<sup>1</sup>, Wanessa Lima de Oliveira<sup>1</sup>, Dilton Martins Pimentel<sup>1</sup> , Gabriel Ali Atta Diab<sup>2</sup>, Ivo Freitas Teixeira<sup>2</sup> , Marcio César Pereira<sup>3</sup> and João Paulo de Mesquita<sup>1,2,\*</sup> 

<sup>1</sup> Department of Chemistry, Federal University of Jequitinhonha and Mucuri Valleys, Rodovia MGT 367—Km 583, n° 5000, Alto da Jacuba, Diamantina 39100-000, MG, Brazil; tais.cruz@ufvjm.edu.br (T.d.S.d.C.); walker.vinicius@ufvjm.edu.br (W.V.F.d.C.B.); ferreira.eduarda@ufvjm.edu.br (E.F.d.O.); wanessa.oliveira@ufvjm.edu.br (W.L.d.O.); dilton.pimentel@ufvjm.edu.br (D.M.P.)

<sup>2</sup> Department of Chemistry, Federal University of São Carlos, Rod. Washington Luís Km 235—SP-310, São Carlos 13565-905, SP, Brazil; gabrieldiab@estudante.ufscar.br (G.A.A.D.); ivo@ufscar.br (I.F.T.)

<sup>3</sup> Instituto de Ciência, Engenharia e Tecnologia, Federal University of Jequitinhonha and Mucuri Valleys, Rua do Cruzeiro, n° 01-Bairro Jardim São Paulo, Teófilo Otoni 39803-371, MG, Brazil; marcio.pereira@ufvjm.edu.br

\* Correspondence: joao.mesquita@ufvjm.edu.br

**Abstract:** Cyamelurate anions obtained from the hydrolysis of polymeric graphitic carbon nitride were used for the preparation of a water-stable and crystalline coordination polymer based on nickel(II)–cyamelurate. The polymer was prepared and applied as a catalyst for the reduction of 4-nitrophenol to 4-aminophenol in the presence of borohydride under ambient conditions. The catalyst was prepared by a simple and environmentally friendly method in an aqueous medium, and it was completely characterized by a variety of techniques, including FTIR, UV–Vis, XRD, TGA, TEM, and STEM. The obtained catalyst was able to catalyze the reaction of 4-nitrophenol to 4-aminophenol with a good kinetic constant. In addition, the catalyst proved to be significantly robust, maintaining a conversion rate greater than 80% after five minutes of reaction for eight consecutive catalytic cycles. In addition, the catalytic activity of the coordination polymer was much higher than that observed for a homogeneous catalyst based on aqueous Ni<sup>2+</sup> ions, suggesting the importance of the structure of the coordination sphere formed by the cyamelurate anions. The results presented here can contribute to the application of other coordination polymers anchored with cyamelurate-like ligands and derivatives, as well as to new catalyst designs based on this coordination site formed by oxygen and nitrogen donor atoms.

**Keywords:** coordination polymer; carbon nitride; cyamelurate; nickel; 4-nitrophenol



**Citation:** Cruz, T.d.S.d.; Batista, W.V.F.d.C.; Oliveira, E.F.d.; Oliveira, W.L.d.; Pimentel, D.M.; Diab, G.A.A.; Teixeira, I.F.; Pereira, M.C.; Mesquita, J.P.d. A Coordination Polymer Based on Nickel(II)–Cyamelurate: A Robust Catalyst with Highly Dispersed Nickel Sites for Nitrophenol Reduction under Ambient Conditions. *C* **2024**, *10*, 27. <https://doi.org/10.3390/c10010027>

Academic Editors: Chi-Hui Tsou, Patrizia Savi and Gil Goncalves

Received: 2 February 2024

Revised: 7 March 2024

Accepted: 14 March 2024

Published: 17 March 2024



**Copyright:** © 2024 by the authors. Licensee MDPI, Basel, Switzerland. This article is an open access article distributed under the terms and conditions of the Creative Commons Attribution (CC BY) license (<https://creativecommons.org/licenses/by/4.0/>).

## 1. Introduction

The process of reducing global carbon emissions will require significant changes in the production sector, which will have a profound impact on the chemical industry. Catalysis will play a central role in this new industrial revolution as it has been estimated that 90% of all commercially produced chemicals go through some catalytic process during at least one stage of their production process. Therefore, catalysts must be redesigned to reduce production costs, minimize dependence on critical minerals, and operate efficiently under ambient conditions [1]. Over the past decade, there has been an increase in the use of coordination polymers (CPs) in various catalytic reactions. The outcomes of these experiments have shown that CPs have the potential to be used as effective heterogeneous catalysts in a range of organic reactions [2]. In fact, catalysts based on coordination polymers are considered very promising, since they are incorporated into the class of single-atom

catalysts [3]. In this field, several reports have demonstrated high activity and performance, especially in recent years [4]. In this context, coordination polymers composed of ligands derived from elements that are abundant in the Earth's crust, which are easy to prepare, low in cost, and physicochemically stable, emerge as interesting alternatives for chemical industry transformation in the coming years. Nevertheless, their availability and certain economic and environmental limitations are barriers to their use in many applications [5].

The cyamelurate anion is a derivative of cyameluric acid for which the nucleus is the C<sub>6</sub>N<sub>7</sub> unit; in addition to its high thermal and chemical stability, this chemical has a conjugated planar structure and high versatility to generate different coordination modes. Due to its N- and O-donors, it enables multitudinous architectures with tunable properties and the possibility of a wide range of lateral chemical modifications [5,6]. As a result, its potential as a ligand has been widely explored in the development of novel hybrid materials for various applications [5,7–11], including the development of a new class of metal-free catalysts for reactions conducted in aqueous media [12,13]. Recently, Wang et al. [12] used potassium cyamelurate as a homogeneous and heterogeneous photocatalyst for the photodegradation of tetracycline hydrochloride under visible-light irradiation in aqueous medium and ethanol, respectively. The authors demonstrated that the degradation efficiency of the molecular structure was approximately 10 times larger than those on melon and g-C<sub>3</sub>N<sub>4</sub>. On the other hand, Oliveira et al. [13] reported on the Fenton-like catalytic behavior of fragments of polymeric g-C<sub>3</sub>N<sub>4</sub> sheets functionalized with cyamelurate-like functional groups. In addition to the good catalytic properties presented by the materials, the authors demonstrated a realistic mechanism for the formation of oxidizing radicals from oxidation and reduction reactions of hydrogen peroxide.

Coordination polymers based on cyamelurate ligands are considered as interesting alternatives, since these molecules can be prepared in aqueous media and have good chemical and thermal stability [9]. Despite the potential of coordination polymers based on the building block derived from s-heptazine, the application of these hybrid materials as heterogeneous catalysts in aqueous media has been poorly reported. Recently, Oliveira et al. [13] prepared and characterized a new coordination polymer formed by iron(III)–cyamelurate units and demonstrated its high performance in the degradation of indigo carmine (IC) dye as a Fenton-like catalyst [7]. On the other hand, this class of materials has been widely used in the detection of nitrophenol [14–17]. However, regarding the use of coordination polymers as catalysts for reduction reactions of nitroaromatic compounds, some papers have recently been published [18–20]. For example, Kuang et al. [18] reported a N-tripodal ligand Cu-based coordination polymer in the presence of N,N-dimethylacetamide (DMA) and water as a catalyst for the reduction reaction of 4-nitrophenol in the presence of NaBH<sub>4</sub> with high catalytic activity. Zang et al. [19] synthesized a new Co-based coordination polymer using a carboxyl–triazolyl bifunctional ligand with good stability in aqueous media. In addition to the excellent catalytic activity in the hydrogenation of 4-nitrophenol under relatively mild conditions, the catalyst was re-used for five cycles without a significant loss of performance. The reduction of 4-nitrophenol (4-NP) to 4-aminophenol (4-AP) has both environmental importance, since it can cause damage to the central nervous system and other organs and tissues, and industrial importance, where it is essential to the manufacture of pharmaceutical products, photographic developers, and corrosion inhibitors, among other applications [21]. Although the reduction reaction of 4-NP to 4-AP ( $E^\circ = -0.76$  V) with NaBH<sub>4</sub> ( $E^\circ = -1.33$  V) is thermodynamically favorable under ambient conditions, this reaction is very slow due to its kinetic barrier, which can be judiciously by-passed through the deployment of a catalyst.

Here, we propose the use of nickel(II)–cyamelurate coordination polymer as a catalyst for the 4-nitrophenol reduction reaction in the presence of sodium borohydride as a reducing agent. We synthesized a stable coordination polymer in an aqueous solution using potassium cyamelurate, an s-heptazine derivative, as a ligand. The resulting material was employed as a heterogeneous catalyst for the hydrogenation reaction of 4-nitrophenol in the presence of NaBH<sub>4</sub> as a reducing agent. The coordination polymer obtained was

characterized by different techniques, and its stability in aqueous media was demonstrated. Finally, we evaluated its catalytic properties and investigated the impact on its structure after catalysis and the likely reaction mechanism.

## 2. Materials and Methods

### 2.1. Materials

All chemicals were purchased and used without further purification. Nickel(II) chloride hexahydrate ( $\text{NiCl}_2 \cdot 6\text{H}_2\text{O}$ ) (Vetec), melamine, and sodium borohydride ( $\text{NaBH}_4$ ) were purchased from Sigma-Aldrich; 4-nitrophenol (4-NP), potassium hydroxide (KOH, 98%), and ethanol were supplied by the company Dinâmica.

### 2.2. Preparation of Materials

Firstly, polymeric  $\text{g-C}_3\text{N}_4$  was obtained from the thermal decomposition of melamine at  $550\text{ }^\circ\text{C}$  in a muffle furnace under a nitrogen atmosphere using a heating ramp of  $3\text{ }^\circ\text{C}\cdot\text{min}^{-1}$  with a plateau of 2 h. Potassium cyamelurate was obtained according to the procedure reported elsewhere by our research group [13]. Briefly, 0.5 g of polymeric  $\text{g-C}_3\text{N}_4$  was dispersed in 40 mL of a 5M KOH aqueous solution using an ultrasound bath. Then, the mixture was refluxed, under stirring, for 6 h at  $80\text{ }^\circ\text{C}$ . After the reaction time, the solution was filtered and washed with ethanol. Finally, the obtained material was dried in an oven ( $60\text{ }^\circ\text{C}$ ) for 24 h. Herein, we use some characterization results of this compound as a complementary/reference form when discussing the results obtained for the nickel(II)–cyamelurate coordination polymer. Nickel(II)–cyamelurate coordination polymer was obtained by dissolving 0.5 g of the material in 50 mL of an aqueous solution of  $\text{NiCl}_2$  with a concentration of  $0.1\text{ mol}\cdot\text{L}^{-1}$  at  $\text{pH}\sim 2$ . The mixture was stirred for 24 h. After this time, the obtained suspension was filtered and the solid washed thoroughly with water until the pH was close to neutrality. To confirm the presence and stability of  $\text{Ni}^{2+}$  ions in the structure of the coordination polymer, 5 mg of nickel(II)–cyamelurate coordination polymer was dispersed in 15 mL of water (solution A). After 15 min of stirring, the solid was separated by filtration and redispersed in another 15 mL of water (dispersion B). To evaluate the presence of  $\text{Ni}^{2+}$  ions in both solutions, drops of a dimethylglyoxime solution (0.1 M) were added to both solution A and solution B.

### 2.3. Characterization of Materials

A Shimadzu diffractometer (XRD6000) was applied to measure the X-ray diffraction (XRD) patterns of the catalysts to evaluate changes in the crystal structure after alkaline hydrolysis and metal ion binding. The XRD data were fitted by the Rietveld method using FullProf Suite 2022 software. The morphology of the samples was characterized by scanning electron microscopy, using a model VEGA3 LMH device (Tescan). The elemental composition and mapping were determined using energy-dispersive X-ray spectroscopy (EDS) equipment (Oxford Instruments) coupled to a microscope. FTIR spectra were obtained with a model IRSPIRIT Shimadzu spectrometer using the single-reflection ATR measurement accessory (QATR-S). Reflectance diffuse data were obtained with a Cary 50 UV–Vis spectrometer (Varian) using a UV–Vis DIFFUSIR diffuse reflection accessory (Pike technologies). TEM images were obtained using a FEI TECNAI G2 F20 operated at 200 kV. The samples ( $\sim 5\text{ mg}\cdot\text{mL}^{-1}$ ) were firstly sonicated with isopropyl alcohol for 5 min and then dropped onto a Cu holey carbon TEM grid. The high-angle annular dark-field scanning transmission electron microscopy (HAADF-STEM) method was used to investigate the dispersion of metal ions across the surface of the material, as well as the possible presence of nanoparticles.

The thermal properties of the materials were investigated using a model 8000 simultaneous thermal analyzer (STA) (Perkin-Elmer) under a  $\text{N}_2$  atmosphere.

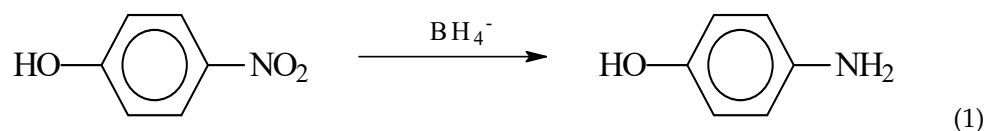
Nickel concentrations were determined using an atomic absorption spectrophotometer, model AA 50B (Varian). It was equipped with a multi-element (Co, Cr, Mn, Fe, Cu, and Ni) hollow cathode lamp (Varian).

The electrochemical activity of the material was investigated using cyclic voltammetry. Electrochemical experiments were obtained in an electrochemical cell using the traditional three-electrode arrangement. Graphite foil and Ag/AgCl electrodes were used as working and reference electrodes, respectively. A Pt wire was used as a counter electrode. Voltammetric data were obtained with a scanning speed of 100 mV/s and a working window of 1.5 to  $-2.0$  V using a  $\mu$ Autolab III potentiostat/galvanostat (Metrohm, Autolab BV) controlled by GPES 4.9 software. All electrochemical measurements were carried out in a 1.0 M NaClO<sub>4</sub> electrolyte solution under ambient conditions. To obtain the cyclic voltammograms of the nickel(II)–cyamelurate CP sample, 200 mL of an aqueous dispersion of the material ( $0.9 \text{ mg}\cdot\text{mL}^{-1}$ ) was directly deposited on the graphite electrode and dried at  $40^\circ\text{C}$ . On the other hand, the cyclic voltammograms of the NiCl<sub>2</sub> sample were obtained with a  $0.12 \text{ mg}\cdot\text{mL}^{-1}$  solution prepared with the supporting electrolyte.

#### 2.4. Catalytic Performance

To evaluate the catalytic activity of nickel(II)–cyamelurate coordination polymer in the reduction reaction of 4-NP (Equation (1)), 100  $\mu\text{L}$  of an aqueous suspension of the material ( $0.9 \text{ mg}\cdot\text{mL}^{-1}$ ) was placed into a quartz cuvette containing 3 mL of a solution containing 4-nitrophenol ( $3 \text{ mg}\cdot\text{L}^{-1}$  or  $0.021 \text{ mM}$ – $6.3 \times 10^{-8}$  moles) and 200  $\mu\text{L}$  of NaBH<sub>4</sub> solution ( $26.4 \text{ mM}$ – $5.28 \times 10^{-6}$  moles). To maintain a consistent concentration throughout the reaction, we employed a relatively high concentration of NaBH<sub>4</sub>, enabling us to conduct a pseudo-first-order kinetic analysis concerning 4-nitrophenol reduction. The rate constant ( $k$ ) of the reduction reaction can therefore be directly calculated from the linear relation between  $\ln(I/I_0)$  and time, where  $I_0$  is the initial absorbance of the reaction system. The kinetics of the reaction were investigated by monitoring the band with maximum absorption at 400 nm by UV–Vis spectroscopy using a Cary 50 instrument (Varian). To assess catalyst reusability, we conducted an eight-cycle recycling experiment in accordance with established literature protocols. After the first reaction cycle, 100  $\mu\text{L}$  was carefully removed from the reaction system, and the concentrations of 4-NP and NaBH<sub>4</sub> were restored through the addition of 100  $\mu\text{L}$  of 4-NP ( $87 \text{ mg}\cdot\text{L}^{-1}$  or  $0.63 \text{ mM}$ ) and 10  $\mu\text{L}$  of NaBH<sub>4</sub> solution ( $26.4 \text{ mM}$ ). For all cycles, the product concentration was determined after 18 min of reaction. All experiments were conducted at room temperature and normal pressure. The adsorption study was conducted similarly to the procedure described for the kinetics of the 4-NP reduction reaction without the addition of the reducing agent and the initial pH of the solution previously adjusted to 10.

In order to investigate the stability of the catalyst and the leaching of the metal after the reaction, a procedure with higher concentrations of reactants and catalyst was carried out. To 20 mL of a 4-nitrophenol solution ( $50 \text{ mg}\cdot\text{L}^{-1}$ ), 15 mg of NaBH<sub>4</sub> and 20 mg of nickel(II)–cyamelurate CP catalyst were added. After complete conversion of 4-NP, i.e., 5 min of reaction, the suspension was quickly filtered and the solid washed thoroughly with water and dried. The turnover frequency (TOF) was determined using this same concentration and volume of the 4-NP solution and 1.5 mg of catalyst.



#### 2.5. Cyclic Voltammetry

Both 4-NP and the reaction product were characterized by cyclic voltammetry. The cyclic voltammograms were obtained in an electrochemical cell using the traditional three-electrode arrangement. The working, reference, and auxiliary electrodes were glassy carbon, Ag/AgCl (saturated), and platinum wire, respectively. To the electrochemical cell, 200  $\mu\text{L}$  of a 4-NP solution ( $50 \text{ mg/L}$ ) dissolved in 600  $\mu\text{L}$  of a Britton–Robinson buffer solution at pH 4, 7, or 10 was added. To obtain the cyclic voltammograms of the reduction reaction

product, i.e., 4-AP, 200  $\mu\text{L}$  was collected after 5 min of the reduction reaction containing 20 mL of a 4-nitrophenol solution ( $50 \text{ mg}\cdot\text{L}^{-1}$ ), 15 mg of  $\text{NaBH}_4$ , and 20 mg of nickel(II)–cyamelurate CP catalyst; afterwards, 600  $\mu\text{L}$  of a Britton–Robinson buffer solution was added to maintain the pH at 4, 7, or 10. Measurements were obtained with a  $\mu\text{Autolab III}$  potentiostat/galvanostat (Metrohm, Autolab BV) controlled by GPES 4.9 software.

### 3. Results

Figure 1A shows images of powdered materials and a schematic illustration of the materials prepared in this research. The X-ray diffraction pattern obtained from the sample containing nickel(II) ions attests to the excellent crystallinity of this material (Figure 1B). A comprehensive analysis, using the Rietveld method, revealed a structure indexed in a triclinic lattice (space group P1,  $Z = 2$ ) with lattice parameters  $a = 14.0223(2) \text{ \AA}$ ,  $b = 23.1364(4) \text{ \AA}$ ,  $c = 15.9773(6) \text{ \AA}$ ,  $\alpha = 15.97^\circ$ ,  $\beta = 152.20^\circ$ ,  $\gamma = 155.99^\circ$ , and unit cell volume  $697.75 \text{ \AA}^3$ .

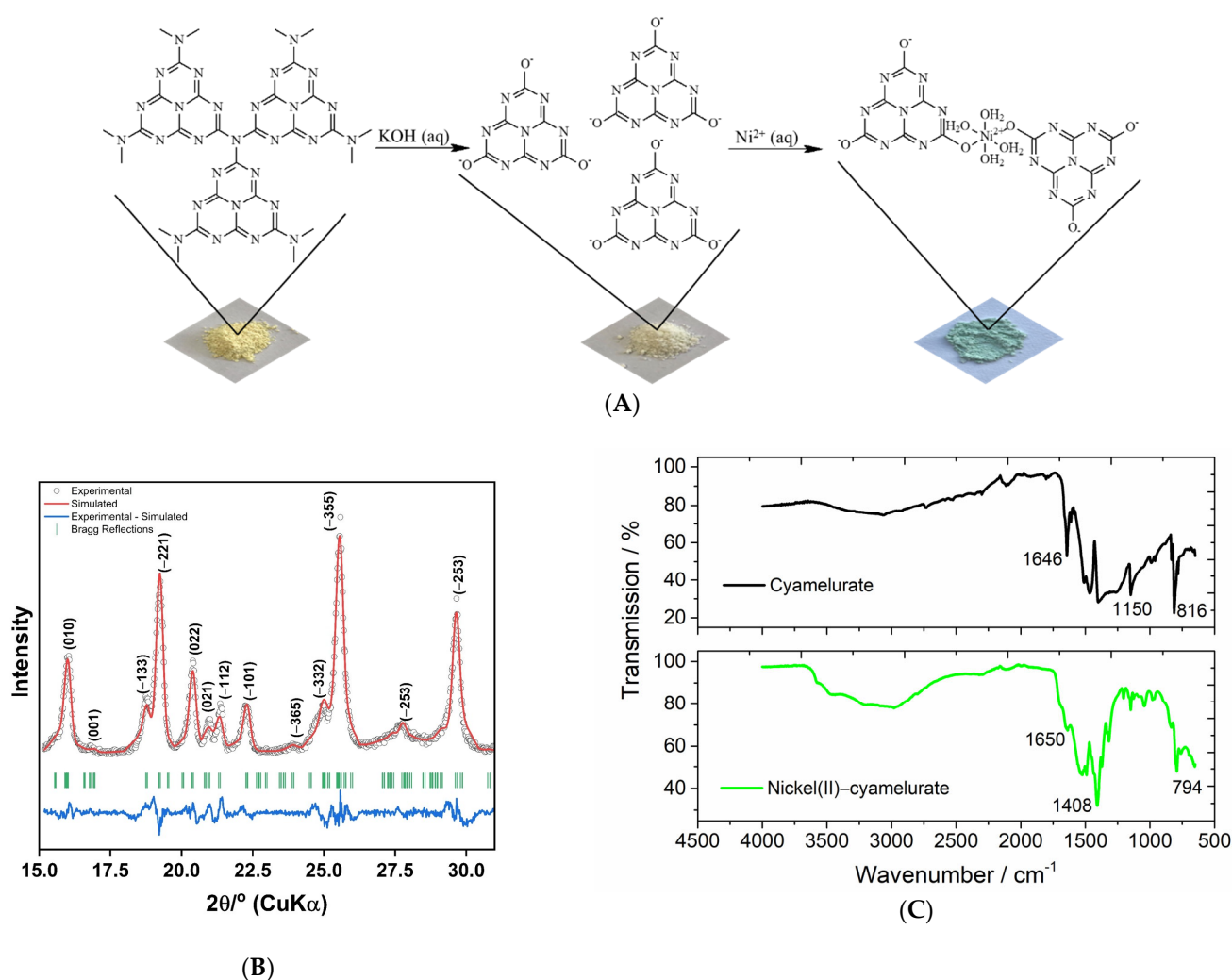


**Figure 1.** (A) Images of powdered materials with schematic illustration of the steps to obtain potassium cyamelurate and the material containing nickel(II) ions. (B) XRD pattern and Rietveld refinements and (C) FTIR spectra obtained for potassium cyamelurate and the coordination polymer based on nickel(II)–cyamelurate.

The unit cell of nickel(II)–cyamelurate displays substantial distortion and asymmetry. The small  $\alpha$  angle indicates a sharp deviation of one crystallographic axis (typically the  $a$ -axis) from orthogonality with the others, leading to a single orientation of nickel atoms and

cyamelurate ligands along this axis. Consequently, atomic positions and bond angles vary along this axis, introducing structural non-uniformity. Additionally, the non-orthogonal  $\beta$  and  $\gamma$  angles induce a rotational distortion in the molecular arrangement within the crystal lattice. This specific angular arrangement results in an asymmetric and distorted structure, leading to diverse bond lengths, bond angles, and coordination environments. These angular distortions are pivotal in shaping the unique structural and chemical characteristics of nickel cyamelurate, contributing to its distinctive properties.

The FTIR spectra are displayed in Figure 1C, from which it can be seen that after the formation of the coordination polymer, the general profile of the FTIR spectrum underwent significant changes compared to the spectrum of potassium cyamelurate. Potassium cyamelurate presents a spectrum with its characteristic bands, especially those centered at 1646 and 816  $\text{cm}^{-1}$ . The first is attributed to the vibrations of the C=N bonds of heterocyclic rings and C=O stretching, and the second is assigned to the ring-sextant out-of-plane bending vibration of the triazine or heptazine rings [22].

After the formation of the coordination polymer, a significant decrease in the band around 1650  $\text{cm}^{-1}$  is observed, indicating the direct participation of these functional groups, i.e., C=O/C-O, in the bonding with metal ions. This change is followed by the shift of the characteristic band of the triazine rings from 816 to 794  $\text{cm}^{-1}$ , indicating a weakening of the bonds in the ligand structure. In addition, the strong absorption at 1408  $\text{cm}^{-1}$  is attributed to, among other bonds, the deformation of OH bonds in the water molecule. The bands located between 930 and 1200  $\text{cm}^{-1}$  are generally associated with the change in metal cations coordinated to structures based on carbon nitrides [23,24].

The SEM images show that after the reaction between potassium cyamelurate and aqueous nickel(II), a drastic change in morphology occurred, with the typical rod shape of cyamelurate being changed to spherical particles, formed by agglomerates of smaller structures similar to wood shavings (Figure 2A–C). The EDS mapping (Figure 2D–I) clearly shows that all monitored elements, including metal ions, were homogeneously dispersed across the entire particle surface of the nickel(II)–cyamelurate CP sample, suggesting the formation of highly dispersed nickel sites. Potassium ions displayed a lower density of spots compared to nickel and other elements, indicating the ion exchange of potassium for nickel during the coordination polymer's preparation. The average elemental composition obtained with this technique is shown in Table S1. The percentage of nickel in the sample was 14.5%. Despite the limitations of the technique, this result is very close to that obtained using the atomic absorption spectroscopy technique, 13.7%, and is in agreement with those previously reported for a coordination polymer based on nickel(II)–cyamelurate [5].

Transmission electronic imaging of the potassium cyamelurate and nickel(II)–cyamelurate CP samples is displayed in Figure 3. As indicated by the SEM images, potassium cyamelurate presents a rod morphology with varying sizes (Figure 3A). Apparently, the rods have a microstructure characterized by the presence of pores homogeneously distributed throughout the structure, with an appearance similar to that of a sponge. This porous nature is likely a result of the fragmentation process induced by KOH. This phenomenon may also have been observed during the partial fragmentation of the polymeric g- $\text{C}_3\text{N}_4$  structure, where the formation of a porous feature in the reduced sheets was similarly observed [7,13]. On the other hand, after the complexation reaction with  $\text{Ni}^{2+}$  ions (Figure 3B), the morphology was predominantly formed by fragmented particles with a more compact structure, as observed by Mohan et al. [5] during their investigation of cyamelurate polymers embedded with several metals.

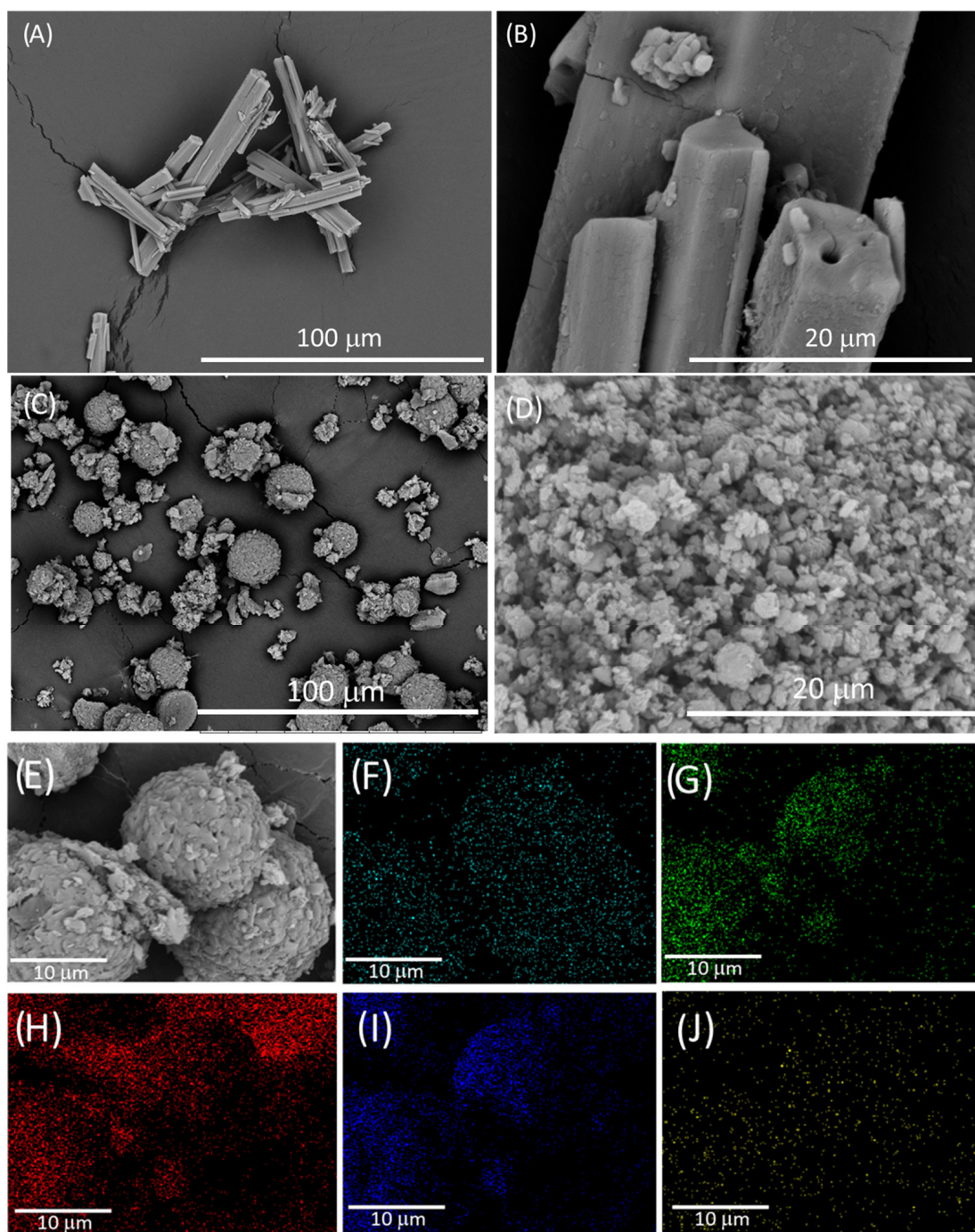


**Figure 2.** SEM images of potassium cyamelurate (A,B) and nickel(II)-cyamelurate CP (C,D). Energy-dispersive spectroscopy (EDS) image (E) and elemental mapping images of Ni (F), N (G), C (H), O (I), and K (J).

To access the potential changes in the nature of Ni sites during the reaction, STEM-HAADF imaging was performed on nickel(II)-cyamelurate, both before and after the reaction (Figure 3C,D, respectively). Initially, the pristine material did not reveal any visible Ni metal formation, indicating a high dispersibility of  $\text{Ni}^{2+}$  species throughout the material. Nevertheless, after the reaction, the formation of small agglomerates (highlighted with green circles) of varying sizes, ranging from 50 to 60 nm, was observed. This suggests the formation of metallic nanoparticles promoted by  $\text{NaBH}_4$  throughout the reaction.

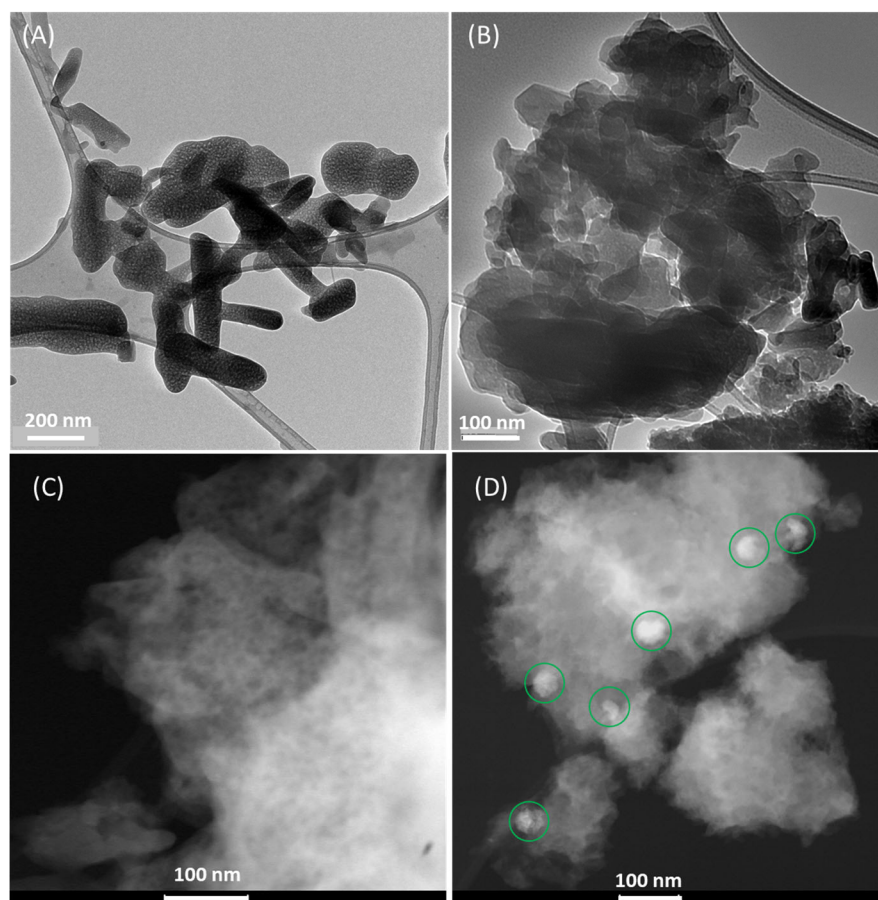


**Figure 3.** TEM images of potassium cyamelurate (A) and nickel(II)-cyamelurate CP (B). STEM-HAADF images of the nickel(II)-cyamelurate CP before (C) and after (D) its use in the catalysis of 4-NP reduction in the presence of  $\text{NaBH}_4$ . Green circles in D indicate the presence of metallic nanostructures.

The thermal properties of nickel(II)-cyamelurate CP were investigated using thermogravimetric analysis, and the results are shown in Figure S1. The coordination polymer presented two mass losses with maxima centered at 196 and 670 °C. The first loss, corresponding to approximately 19%, is attributed to the elimination of water molecules chemically bonded to the metal, while the second, corresponding to 56% of the total mass, is attributed to the decomposition of the organic structure, i.e., cyamelurate anions. The presence of structural water molecules, as labile ligands, is interesting for catalytic activity, since the ligands attached to catalytically active metal ions impact on the reaction rate [25], and inert ligands can hinder the access of the reagent to the catalytic site. The residual mass of approximately 25% is associated with the formation of nickel oxide and waste carbon materials after the decomposition of the organic structures.

The electronic properties of potassium cyamelurate and nickel(II)-cyamelurate CP were analyzed by UV-Vis spectroscopy and cyclic voltammetry (Figures S2 and S3). Polymeric  $g\text{-C}_3\text{N}_4$  presents a typical UV-Vis spectrum with a strong absorption from 440 nm. After hydrolysis, that is, the formation of cyamelurate anions, the conjugation between the structure of the *s*-heptazine units is broken, causing a blue shift at the beginning of absorption (440 → 400 nm). After the coordination of nickel(II) ions, a shift towards the absorption associated with the structure of the  $\text{C}_6\text{N}_7$  nucleus of both polymeric  $g\text{-C}_3\text{N}_4$  and cyamelurate was observed. For the polymeric  $g\text{-C}_3\text{N}_4$  the shift was from 440 to 430 nm, and for the cyamelurate anions, a more significant shift was observed, from 400 to 360 nm. For the nickel(II)-cyamelurate sample, an absorption located between 600 and 800 nm was also observed, typically associated with hydrated nickel(II) complexes.

The electrochemical properties in aqueous media of the nickel(II)–cyamelurate CP were studied by cyclic voltammetry. Figure S3 shows the cyclic voltammograms obtained in the presence of 0.1 M NaClO<sub>4</sub> as the supporting electrolyte. The coordination polymer presents two well-defined redox processes at 0.7 V and 0.51 V vs. Ag/AgCl at circumneutral pH. The redox potential obtained, 0.60 V, is similar to the redox potential of the Ni<sup>2+</sup> solution (0.55 V) and very close to the redox potential of the reaction Ni<sup>2+</sup> + 2e<sup>-</sup> → Ni(0), E = 0.45 V vs. Ag/AgCl. In general, both UV–Vis spectroscopy and the results obtained through cyclic voltammetry suggest an electronic structure of the coordination polymer similar to that observed for water–nickel(II) complexes.

The results shown so far, in particular the high dispersibility and structural and electronic homogeneity of the coordination sphere of the metal centers, enable the use of this class of materials as catalysts for a variety of reactions.

#### *Catalytic Performance in the Reduction of 4-Nitrophenol*

One of the main challenges associated with the use of coordination polymers in catalytic processes is their structural stability in the presence of a solvent, especially water [26]. We conducted a simple qualitative test using the typical complexation reaction between dimethylglyoxime (DMG) and nickel(II) ions to evaluate the stability of the coordination polymer in water. In this case, a low chemical stability of the material would lead to the leaching of Ni<sup>2+</sup> ions due to the replacement of the cyamelurate ligands by water molecules, which would be detected by the formation of a compound with a reddish color. In Figure 4, images of the solutions containing DMG are shown. Figure 4A shows the supernatant solution after separation of the solid and the addition of DMG. As can be seen, the solution remained colorless after the addition of the complexing agent (nickel(II) reacts with DMG, forming reddish complexes), indicating a low solubility and good structural stability of the compound, without an indication of nickel leaching under the reaction conditions. On the other hand, when DMG was added in the presence of the nickel(II)–cyamelurate coordination polymer, there was a clearly observable color change in the solution (Figure 4B,C), indicating the alteration of the coordination sphere of the metallic center due to the replacement of water molecules by DMG.

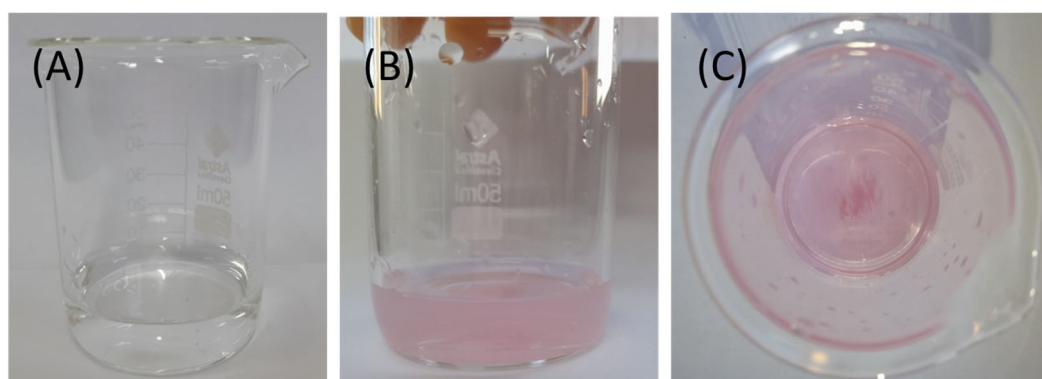


**Figure 4.** (A) Image of the supernatant solution obtained after the separation of the nickel(II)–cyamelurate CP added with DMG. Images of the addition of DMG in the presence of the nickel(II)–cyamelurate solid: (B) side view and (C) top view.

Once the stability of the coordination polymer based on nickel(II)–cyamelurate had been demonstrated, the catalytic properties were evaluated through the reduction of 4-nitrophenol (4-NP) in the presence of sodium borohydride. The 4-NP presents a strong absorption in the UV region of the spectrum, more precisely at 317 nm [27]. However, at pH values greater than 7.15, the pK<sub>a</sub> of 4-NP, the predominant structure is the 4-nitrophenolate anion, which has a yellow color and a maximum absorption at 400 nm. Therefore, when evaluating the reduction reaction of 4-nitrophenolate to 4-aminophenol, it is important

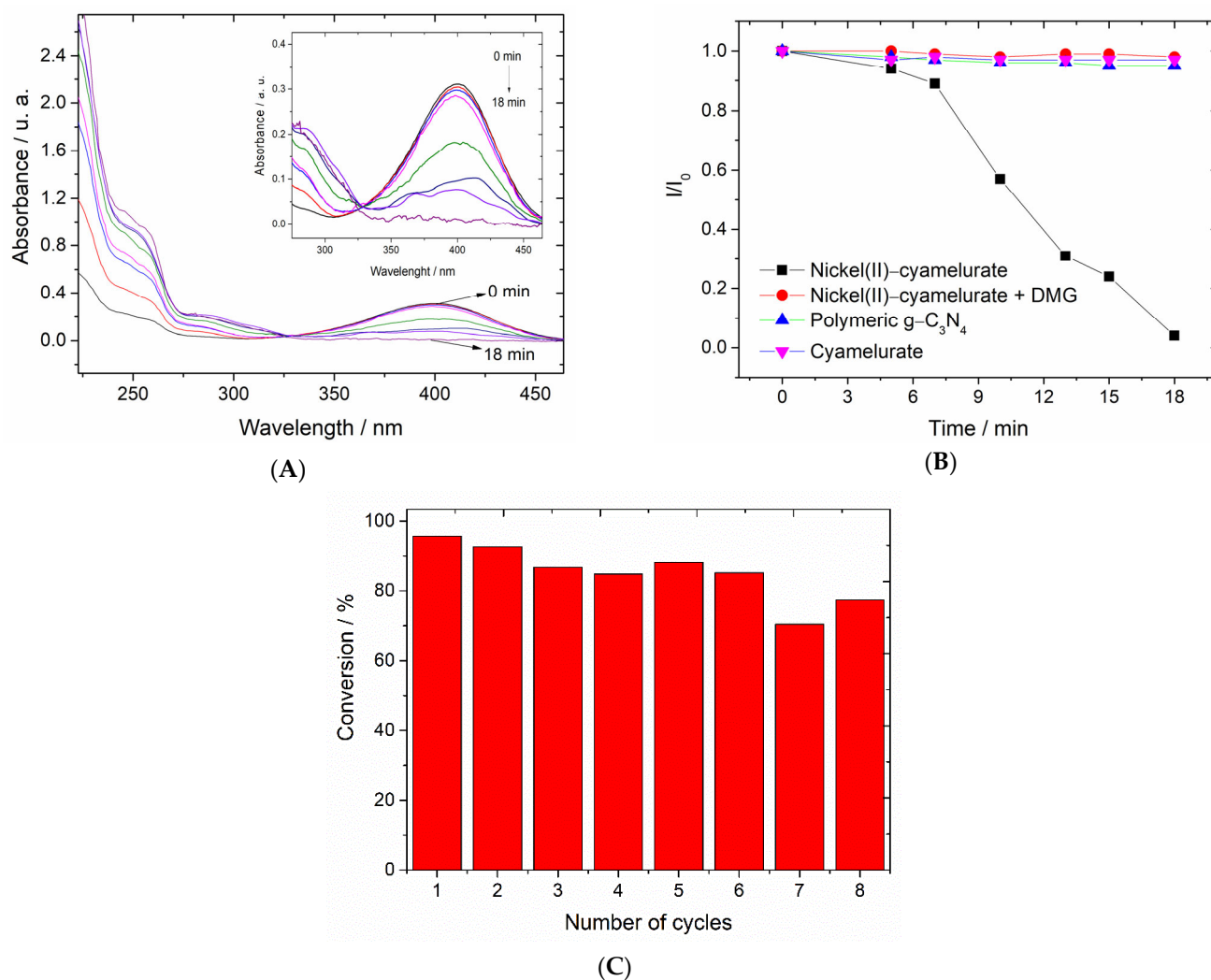
to consider the pH of the system in the presence of the catalyst. A decrease in pH to a value close to 7 will lead to a shift in the equilibrium of the 4-nitrophenolate anion, causing the absorption at 400 nm to shift towards the protonated structure of 4-NP, which absorbs at 317 nm. This evaluation is particularly important, since the product of the 4-NP reduction reaction, 4-aminophenol, has a maximum absorption close to 300 nm. Therefore, the decrease in pH after the addition of the catalyst may indicate a non-existent reduction reaction. Here, after the addition of NaBH<sub>4</sub> to 4-NP solution, the color turned from colorless to bright yellow, accompanied by the change in pH from 5.8 to 10.0. Then, the nickel(II)–cyamelurate CP catalyst was added to the system, and the pH underwent a small change to 9.8. Under these conditions, the decrease in absorption at 400 nm and, in parallel, the increase in adsorption at ~290 nm, associated with the reduction reaction product (4-AP), can be monitored by UV–Vis spectroscopy.

Figure 5A displays the time-dependent UV–Vis spectra, in which the decrease in absorption at 400 nm, attributed to the 4-nitrophenolate ion, can be seen. This decrease is accompanied by an increase in absorption at around 290 nm, characteristic of the 4-AP compound. In Figure S4, the time-dependent UV–Vis spectra are shown for the system containing only the catalyst and the 4-NP (adsorption) with the initial pH of the 4-NP solution adjusted to 10. As can be seen, after a time of 18 min, the absorption maximum at 400 nm remained unchanged. The possible reductive catalytic properties of the precursor materials, i.e., polymeric g-C<sub>3</sub>N<sub>4</sub> and cyamelurate, were also evaluated. The spectra obtained for 4-NP in the presence of these materials are shown in Figure S4C,D. Again, no decrease in absorption centered at 400 nm was observed, indicating the inability of these materials to catalyze the 4-NP reduction reaction in the presence of borohydride. Similar results were obtained in the presence of a homogeneous catalyst prepared with the same concentration of nickel(II) ions (Figure S4E). This result indicates that, regardless of the reaction mechanism involved during the progress of the reaction, the unique structure of the coordination polymer has a determining role in the reaction kinetics. Another interesting result is that in the presence of dimethylglyoxime (DMG), a typical Ni<sup>2+</sup> complexing agent, all kinetic activity of the coordination polymer was strongly inhibited (Figure S4F).

In Figure 5B, the results show the relative absorption intensity at 400 nm over time for all materials evaluated. Differently from the coordination polymer, polymeric g-C<sub>3</sub>N<sub>4</sub> and cyamelurate samples showed negligible reductions of 8% and 3%, respectively. On the other hand, the nickel(II)–cyamelurate CP sample showed a reduction in absorption greater than 90% after 18 min of reaction, indicating a good catalytic activity for the conversion of 4-NP into 4-AP. Since the concentration of NaBH<sub>4</sub> in the reaction system is much higher compared to that of 4-NP, the pseudo-first-order kinetic model was applied to estimate the rate constants (K) for 4-NP hydrogenation [19]. The estimated result was  $0.068 \pm 0.01 \text{ min}^{-1}$ , with a corresponding TOF of  $5 \text{ h}^{-1}$ .

It is also possible to observe from the relative intensity data a latency time of approximately 5 min after the catalyst introduction, followed by the rapid conversion of 4-NP. Several hypotheses have been reported regarding this latency [28]. This result suggests a previous “activation” step, for example, the reduction of Ni<sup>2+</sup> ions to Ni(0), followed by the dissociative adsorption of hydrogen molecules or even activation through the replacement of labile ligands, i.e., H<sub>2</sub>O by H<sup>+</sup> ions.

The results of the reusability test on nickel(II)–cyamelurate CP are shown in Figure 5C. Overall, the catalyst proved to be quite robust, maintaining its conversion capacity at above 80% even after eight reaction cycles. The small loss of catalytic activity may be associated with the reduction of Ni<sup>2+</sup> ions with the formation of nanoparticles and subsequent coalescence leading to the formation of larger structures with low catalytic activity. On the other hand, the investigation of the supernatant solution showed a small concentration of Ni<sup>2+</sup> ions, 0.36% wt., suggesting metal leaching during the reaction, which may also contribute to this decrease in catalytic activity.



**Figure 5.** (A) Time-dependent UV–Vis spectra obtained for 4-NP solution in the presence of the nickel(II)–cyamelurate CP and borohydride. (B) Conversion kinetics of 4-NP to 4-AP. (C) Cycles of reusability of nickel(II)–cyamelurate for the reduction of 4-NP in the presence of NaBH<sub>4</sub>. Experimental conditions: initial pH = 10, catalyst mass = 0.09 mg, [4-NP] = 3 mg L<sup>-1</sup>, and NaBH<sub>4</sub> mass = 0.2 mg.

To investigate the reaction products formed after the reaction, cycle voltammograms were obtained at acidic, circumneutral, and basic pH. Figure 6 shows the cyclic voltammograms obtained for 4-NP before and after 5 min of reaction in the presence of NaBH<sub>4</sub> and nickel(II)–cyamelurate CP catalyst in Britton–Robinson buffer solution at different pH values. Unlike the results in acidic and circumneutral environments, the cyclic voltammograms obtained in alkaline pH present a higher capacitance current, causing lesser definition of the redox peaks, especially in relation to the results presented for the product of the 4-NP reduction reaction (Figure 6C). In general, small changes in the positions of potential peaks in the region around 0.0 V (Ag/AgCl) were still observed. On the other hand, a well-defined shift in the reduction potential can be attributed to the functional group –NO<sub>2</sub>, from –0.75 to –0.93 V from the acidic to the alkaline medium. The reduction peak centered in this region corresponds to the reduction of four electrons of the nitro group that results in the formation of hydroxylamine [29]. The cyclic voltammograms of the 4-NP sample presented a redox couple positioned above 0 V, which were also associated to the oxidation/reduction of the nitro function [30,31]. Using a glassy carbon electrode and under acidic conditions, the oxidation peak attributed to the –OH functional group is normally observed at potentials close to 1 V [30]. After the reaction, the intense reduction peak characteristic of the –NO<sub>2</sub> function completely disappeared, indicating a

chemical modification of the molecule. In addition, from the electrochemical data of the reaction product, we observed a reversible redox reaction that was well defined in neutral and acidic media, at potentials slightly lower than 0 V(Ag/AgCl). The absence of other oxidation and reduction peaks in the voltammograms obtained for the 4-NP sample after the reduction reaction suggests the presence of very low concentrations of the reagent or even intermediate compounds eventually formed from the reduction of nitro groups, such as hydroxylamine functional groups and other molecules.

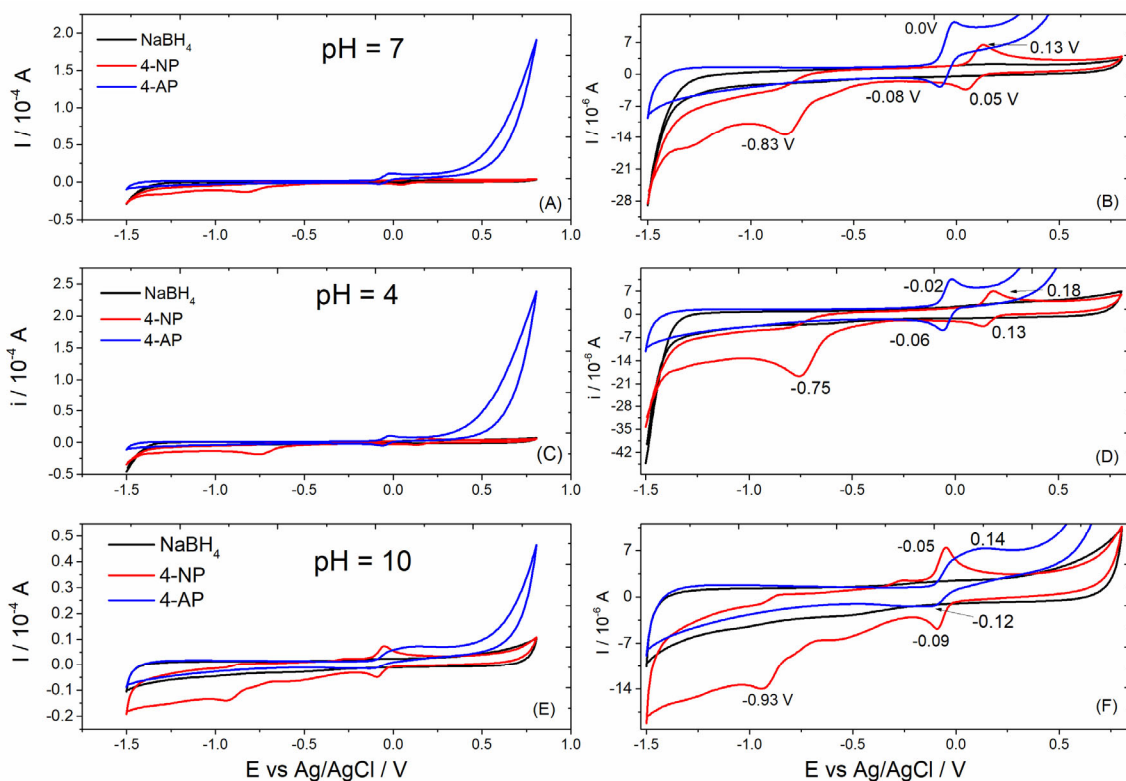


**Figure 6.** Cyclic voltammograms obtained for NaBH<sub>4</sub> and 4-NP solutions before and after (4-AP) the reaction catalyzed by nickel(II)-cyamelurate CP at different pH values. (A,C,E) show the voltammograms obtained in the potential window from  $-1.5$  to  $0.8$  V, while (B,D,F) are the respective magnifications.

#### 4. Discussion

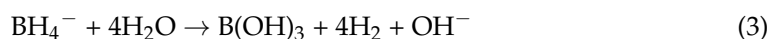
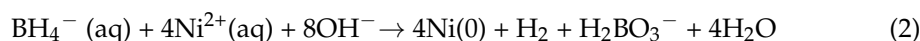
In the presence of a strongly alkaline medium, the N-C bonds of tertiary and, eventually, secondary and primary amines, formed by the incomplete condensation of nitrogenous precursors in polymeric g-C<sub>3</sub>N<sub>4</sub>, are hydrolyzed with the elimination of ammonia molecules, leading to the formation of cyamelurate anions with low concentrations of impurities [13]. Upon the addition of cyamelurate anions to a Ni<sup>2+</sup> solution, a greenish solid promptly forms, indicating the creation of coordinated structures featuring hydrated Ni<sup>2+</sup> ions (see Figure 1A). As a result of the electronic and structural characteristics of the cyamelurate ligand, a coordination polymer with good stability was formed in aqueous media, allowing for its use in various applications under these conditions. Here, we propose its use as a catalyst for the traditional nitrophenol reduction reaction. The high dispersibility of the metal ions associated with the electronic/structural homogeneity of the catalytic site, together with a suitable interface for interaction between the reagents in addition to the surface of the catalyst, provided by the organic structure of the ligand, indicates a catalyst with properties suitable for reduction reactions [29].

Our main hypothesis for the reaction mechanism consists in the formation of Ni(0) sites through the reaction between Ni<sup>2+</sup> ions and the strong reducing agent BH<sub>4</sub><sup>-</sup>. In Fig-

ure S5, images and UV–Vis spectra of the aqueous Ni(II) and nickel(II)–cyamelurate CP solution/suspension are shown before and after 18 min of reaction with sodium borohydride. From the images, it is possible to clearly observe the presence of dark colored particles dispersed in both solutions, but this is much more evident in the aqueous Ni<sup>2+</sup> sample. The UV–Vis spectrum of this sample (Figure S5) clearly shows the disappearance of the typical absorption bands of [Ni(H<sub>2</sub>O)<sub>6</sub>]<sup>2+</sup> around 700 and 400 nm, generating a noisy plasmon resonance spectrum of metallic nanoparticles [30]. On the other hand, the nickel(II)–cyamelurate CP catalyst was separated by the filtration method to check its structural integrity and verify the presence of nickel(II) ions after its catalytic performance. Figure S6 shows the images of the aqueous dispersion of the material recovered in the presence of DMG. As can be clearly seen, as in the tests to verify the aqueous stability of nickel(II)–cyamelurate CP, the reddish color indicates that Ni<sup>2+</sup> ions were present in the material. In addition, the FTIR spectra obtained before and after using the material as a catalyst in the 4-NP reduction reaction are very similar (Figure S7), suggesting the maintenance of the basic structure of the compound, formed by cyamelurate and hydrated Ni<sup>2+</sup> ions. However, the percentage of nickel in the sample after use as a catalyst in the reaction increased significantly, from 14.5 to 33% wt. These results indicate that part of the nickel ions can be reduced in the presence of a strong reducing agent, forming small clusters and/or nickel nanoparticles with the leaching of organic ligand molecules. The presence of nickel metal was confirmed using cyclic voltammetry (Figure S8). The cyclic voltammogram of the material obtained after the reaction clearly presents two redox peaks associated with the Ni<sup>2+</sup>/Ni(0) couple at 0.78 V and 0.88 V vs. saturated Ag/AgCl. Qualitative testing using molecular iodine also showed the presence of reduced nickel species. STEM-HAADF imaging of the nickel(II)–cyamelurate CP after its use in the catalysis of 4-NP reduction in the presence of NaBH<sub>4</sub> clearly shows the presence of metallic nanoparticles anchored to the surface of the material (Figure 3D).

The reduction reaction of nitroaromatic compounds can follow a direct pathway, involving the formation of intermediates such as nitrous and N-phenylhydroxylamine, or a condensation pathway, with the formation of intermediates containing azo groups [31]. In the presence of a catalyst, currently, two main mechanisms for the reduction of nitroarenes using metal-based catalysts have been proposed [32,33]. The first, based on metallic nanomaterials such as Pt, Pd, and Ni, involves the adsorption of both reactants on the surface of the nanoparticle [32]; the second is based on the heterolytic cleavage of hydrogen molecules [33]. For a homogeneous catalyst, it is clear that the catalytic process basically involves the reduction of Ni<sup>2+</sup> ions and the subsequent reduction reaction on its surface—a relatively slow process (see Figure S4E). On the other hand, we observed the following results for the nickel(II)–cyamelurate CP catalyst: (i) a latency time of approximately five minutes; (ii) fast conversion kinetics compared to the homogeneous catalyst; (iii) inhibition of the reaction in the presence of DMG; (iv) the presence of nickel(II) ions after the reduction reaction, in addition to its basic structure formed by cyamelurate anions and water molecules; and (v) the formation of metallic nanoparticles. It is clear that the structure of the coordination polymer is important for the catalytic process, since the reaction kinetics are much higher in relation to those for the homogenous catalyst. This suggests that part of the nickel sites in the coordination polymer might be reduced to Ni(0) and, in a lesser proportion, form clusters and/or nanoparticles. However, they remain predominantly dispersed, explaining the high activity compared with the nanoparticles formed by the reduction of Ni<sup>2+</sup> salt. Some authors have carried out detailed structural characterizations of coordination polymers composed of cyamelurate and certain transition metals, such as nickel(II). The studies, which included single-crystal X-ray diffraction, indicate that metal–organic polymers made of nickel(II)–cyamelurate have two metal ions in each unit cell. One of these is coordinated by cyamelurate anions and water molecules, and the other has a coordination sphere formed by six water molecules. We speculate that in the presence of a strong reducing agent, the [Ni(H<sub>2</sub>O)<sub>6</sub>]<sup>2+</sup> site could be reduced more effectively, leading to the formation of metallic nanostructures while the nickel(II) coordinated by

the organic ligand remains with its electronic structure unchanged or is reduced to Ni(0), which remains “stabilized” and highly dispersed across the surface. It seems that this system does not involve a single reactional process. On the other hand, the presence of organic ligands can improve the interaction between 4-NP molecules, thus facilitating their adsorption on the surface of the material. Finally, it is necessary to consider the fact that in the presence of the complexing agent DMG, the catalyst is completely inactivated, due to “blocking” of the nickel sites. Thus, the reaction mechanism must initially involve the reaction of  $\text{NaBH}_4$  with  $\text{Ni}^{2+}$  ions, forming, as its products, reduced and predominantly dispersed nickel species and hydrogen gas, which is activated on the reduced metallic sites. This is a catalytic process through the dissociative adsorption of reagents [31]. In other words, at first,  $\text{BH}_4^-$  reacts with nickel ions, forming reduced nickel species (Equation (2)), with the majority remaining highly dispersed and others coalescing and forming metallic nanoparticles. In this reaction between borohydride and water (Equation (3)), hydrogen molecules are formed, which are adsorbed and activated on the surface of the metallic structures that subsequently react with 4-NP to form 4-AP.



## 5. Future Perspectives

The development of new catalysts with high atomic efficiency is very promising for sustainable catalytic systems. Together with other classes of materials, coordination polymers with good stability in aqueous systems are extremely relevant materials, due to the greater ease of the structural and electronic control of the catalytic site compared to that for other supports for metal ions. Specifically, regarding structures based on the *s*-heptazine unit, i.e., cyamelurate, the ease of obtaining them and their physicochemical stability are differentiating factors for the use of these materials as ligands. At this moment, there are few reports on the use of this class of compounds as an alternative for the development of high-efficiency catalysts. Thus, new materials prepared with different metals and mixed structures should be reported in the short term. On the other hand, proposals for selective modification of the ligand structure to optimize the characteristics of the catalytic site and increase the stability of the coordinated metal will be of great interest, in addition to the investigation of cationic mechanisms in different reaction processes, which are among the most relevant future perspectives for these materials.

## 6. Conclusions

A water-stable and crystalline coordination polymer based on nickel(II)–cyamelurate was obtained by a simple and environmentally friendly method in an aqueous medium. The prepared material was applied as a catalyst for the reduction of 4-nitrophenol in the presence of borohydride under ambient conditions. Rietveld refinement revealed a distorted triclinic unit cell with lattice parameters  $a = 14.0223(2) \text{ \AA}$ ,  $b = 23.1364(4) \text{ \AA}$ ,  $c = 15.9773(6) \text{ \AA}$ ,  $\alpha = 15.97^\circ$ ,  $\beta = 152.20^\circ$ ,  $\gamma = 155.99^\circ$ , and volume  $697.75 \text{ \AA}^3$ . Because of its high structural stability in aqueous media, the catalyst was used for the reduction reaction of 4-nitrophenol to 4-aminophenol. In addition to its good kinetic constant,  $0.068 \pm 0.01 \text{ min}^{-1}$ , the catalyst proved to be significantly robust, maintaining a conversion rate greater than 80% after eight consecutive catalytic cycles. On the other hand, the catalytic activity of the coordination polymer was much higher than that observed for a homogeneous catalyst based on aqueous  $\text{Ni}^{2+}$  ions, suggesting the importance of the structure of the coordination sphere formed by the cyamelurate anions. This can be explained by the uniform distribution of the metallic ions, in parallel with the high accessibility and electronic and structural homogeneity of the catalytically active sites. Finally, the results presented herein can contribute to the design of new catalysts with highly dispersed metal ions anchored on coordination sites based on the cyamelurate-like functional groups.

**Supplementary Materials:** The following supporting information can be downloaded at: <https://www.mdpi.com/article/10.3390/c10010027/s1>, Table S1. Elemental composition obtained for nickel(II)-cyamelurate CP and MOP-3 reported by Mohan et al. Figure S1, Thermogravimetric analysis (TGA) and derivative thermogravimetric (DTG) obtained for polymeric g-C<sub>3</sub>N<sub>4</sub> and nickel(II)-cyamelurate CP, Figure S2. DRS spectra (A) and Kubelka-Munk absorbance (B) obtained from polymeric g-C<sub>3</sub>N<sub>4</sub>, polymeric g-C<sub>3</sub>N<sub>4</sub>+Ni<sup>2+</sup>, cyamelurate and nickel(II)-cyamelurate CP. Inset in B): amplification of the absorbance of the region located between 600 and 800 nm, Figure S3. Cyclic voltammograms obtained for nickel(II)-cyamelurate CP and aqueous NiCl<sub>2</sub> solution, Figure S4. Time-dependent UV-Vis spectra obtained for 4-NP solution in the presence of the nickel(II)-cyamelurate CP and borohydride (A), in the presence of only the nickel(II)-cyamelurate CP catalyst (B). In (B) the initial pH of the solution was adjusted to 10. 4-NP solution in the presence of the borohydride and C) polymeric g-C<sub>3</sub>N<sub>4</sub> and D) cyamelurate. In (D), the high absorption from 325 nm is caused by cyamelurate. (E) 4-NP solution in the presence of the NiCl<sub>2</sub> and borohydride. (F) 4-NP solution in the presence of the nickel(II)-cyamelurate CP, borohydride and dimethylglyoxime (DMG), Figure S5. UV-Vis spectra obtained for NiCl<sub>2</sub> solution (A) and nickel(II) cyamelurate CP dispersion (B) before and after 18 min of reaction with NaBH<sub>4</sub>. Figure S6. Digital images of suspensions containing nickel (II)-cyamelurate CP before (A) and after (B) reduction reaction of 4-nitrofenol. Figure S7. FTIR Spectra obtained for the catalyst before and after the catalytic tests in the presence of sodium borohydride. The spectra were obtained in IRSPIRIT equipment (Shimadzu) using the Single Reflection ATR measurement accessory (QATR-S). Figure S8. Cyclic voltammograms obtained for the nickel(II)-cyamelurate CP catalyst after use in the 4-NP reduction reaction in the presence of NaBH<sub>4</sub>. The traditional three-electrode system was used in the experiment using as reference an Ag/AgCl electrode saturated with KCl and a platinum wire counter electrode. The working electrode was prepared by depositing 10uL of a suspension (1mg/mL) of the material on the surface of a glassy carbon electrode. 0.1M NaClO<sub>4</sub> was used as supporting electrolyte. The arrow indicates the scanning direction. The results shown refer to the first scan within the potential window from 0 to 1.4V.

**Author Contributions:** Conceptualization, T.d.S.d.C., E.F.d.O. and J.P.d.M.; methodology, T.d.S.d.C., E.F.d.O., G.A.A.D., D.M.P., W.V.F.d.C.B. and W.L.d.O.; validation, T.d.S.d.C., E.F.d.O., G.A.A.D., W.V.F.d.C.B. and W.L.d.O.; formal analysis, T.d.S.d.C., E.F.d.O., G.A.A.D., W.V.F.d.C.B. and W.L.d.O.; investigation, T.d.S.d.C., E.F.d.O., G.A.A.D., W.V.F.d.C.B. and W.L.d.O.; resources, J.P.d.M.; data curation, T.d.S.d.C., E.F.d.O., G.A.A.D., W.V.F.d.C.B. and W.L.d.O.; writing—original draft preparation, T.d.S.d.C., E.F.d.O., G.A.A.D. and J.P.d.M.; writing—review and editing, J.P.d.M., I.F.T. and M.C.P.; supervision, J.P.d.M.; funding acquisition, J.P.d.M. and I.F.T. All authors have read and agreed to the published version of the manuscript.

**Funding:** The authors acknowledge LMMA and the support from MULTIFAR. This research was financially supported by the Brazilian funding agencies CAPES 001, CNPq (102190/2022-4, 423196/2018-9, 403064/2021-0, and 405752/2022-9), FAPEMIG (APQ-00370-22, APQ-003088-21, and APQ-02629-17), and FAPESP (2020/14741-6, 2021/13271-9, 2022/16273-5, 2021/12394-0, 2021/14006-7, and 2021/11162-8).

**Data Availability Statement:** The data presented in this study are available from the authors.

**Conflicts of Interest:** The authors declare no conflicts of interest.

## References

1. Centi, G. Smart catalytic materials for energy transition. *SmartMat* **2020**, *1*, e1005. [[CrossRef](#)]
2. Yan, H.; Su, C.; He, J.; Chen, W. Single-atom catalysts and their applications in organic chemistry. *J. Mater. Chem. A* **2018**, *6*, 8793–8814. [[CrossRef](#)]
3. Kaiser, S.K.; Chen, Z.; Akl, D.F.; Mitchell, S.; Pérez-Ramírez, J. Single-Atom Catalysts across the Periodic Table. *Chem. Rev.* **2020**, *120*, 11703–11809. [[CrossRef](#)]
4. Singh, B.V.; Sharma, V.; Gaikwad, R.P.; Fornasiero, P.; Zbořil, R.; Gawande, M.B. Single-Atom Catalysts: A Sustainable Pathway for the Advanced Catalytic Applications. *Small* **2021**, *17*, 2006473. [[CrossRef](#)]
5. Mohan, M.; Rajak, S.; Tremblay, A.A.; Maris, T.; Duong, A. Syntheses of mono and bimetallic cyamelurate polymers with reversible chromic behaviour. *Dalton Trans.* **2019**, *48*, 7006–7014. [[CrossRef](#)]
6. Schwarzer, A.; Saplinova, T.; Kroke, E. Tri-s-triazines (s-heptazines)—From a “mystery molecule” to industrially relevant carbon nitride materials. *Coord. Chem. Rev.* **2013**, *257*, 2032–2062. [[CrossRef](#)]

7. de Oliveira, W.L.; de Oliveira, E.F.; da Cruz, T.D.S.; Batista, W.V.F.D.C.; Moraes, C.; Pereira, F.V.; Forim, M.R.; Atta Diab, G.A.; Teixeira, I.F.; Pereira, M.C.; et al. Preparation and Characterization of a Coordination Polymer Based on Iron (III)-Cyamelurate as a Superior Catalyst for Heterogeneous Fenton-Like Processes. *Langmuir* **2023**, *39*, 5002–5011. [[CrossRef](#)] [[PubMed](#)]
8. Zhang, X.; Du, X.; Wang, J.; Wang, F.; Liang, F.; Hu, Z.; Lin, Z.; Wu, Y.  $K_3C_6N_7O_3 \cdot 2H_2O$ : A Multifunctional Nonlinear Optical Cyamelurate Crystal with Colossal  $\pi$ -Conjugated Orbitals. *ACS Appl. Mater. Interfaces* **2022**, *14*, 53074–53080. [[CrossRef](#)]
9. Horvath-Bordon, E.; Kroke, E.; Svoboda, I.; Fueß, H.; Riedel, R.; Neeraj, S.; Cheetham, A.K. Alkalicymelurates,  $M_3[C_6N_7O_3] \cdot xH_2O$ ,  $M = Li, Na, K, Rb, Cs$ : UV-luminescent and thermally very stable ionic tri-s-triazine derivatives. *Dalton Trans.* **2004**, *22*, 3900–3908. [[CrossRef](#)]
10. Essalhi, M.; Mohan, M.; Dissem, N.; Ferhi, N.; Abidi, A.; Maris, T.; Duong, A. Two different pore architectures of cyamelurate-based metal–organic frameworks for highly selective  $CO_2$  capture under ambient conditions. *Inorg. Chem. Front.* **2023**, *10*, 1037–1048. [[CrossRef](#)]
11. Mohan, M.; Essalhi, M.; Durette, D.; Rana, L.K.; Ayevide, F.K.; Maris, T.; Duong, A. A Rational Design of Microporous Nitrogen-Rich Lanthanide Metal–Organic Frameworks for  $CO_2/CH_4$  Separation. *ACS Appl. Mater. Interfaces* **2020**, *12*, 50619–50627. [[CrossRef](#)]
12. Wang, W.; Chen, Z.; Yang, X.; Audebert, P.; Sahoo, S.; Chen, J.; Liu, Y.; Alpay, S.P.; Xie, L. Wei Potassium cyamelurate  $K_3[C_6N_7O_3]$  rod: A new visible-light photocatalyst for homogeneous/heterogeneous degradation of antibiotics. *Appl. Catal. A Gen.* **2022**, *641*, 118669. [[CrossRef](#)]
13. Oliveira, W.L.; de Oliveira, E.F.; do Carmo Batista, W.V.F.; Mourão, H.A.; Pires, M.J.M.; Coelho, R.M.; Diab, G.A.A.; Teixeira, I.F.; Marques, G.; Mastelaro, V.R.; et al. A metal-free catalyst based on g- $C_3N_4$  functionalized with cyamelurate-like groups: Catalytic properties and mechanism of a new heterogeneous Fenton-like catalyst. *Carbon* **2023**, *214*, 118366. [[CrossRef](#)]
14. Hu, Z.; Luo, R.; Wang, S.H.; Zhang, N.; Chen, C. Two Metal–Organic Coordination Polymer for Fluorescence Detection of 4-Nitrophenol. *Chin. J. Inorg. Chem.* **2019**, *35*, 1586–1592.
15. Xu, X.Y.; Cui, H.L.; Liu, W.; Chen, X.L.; Yang, H.; Liu, L.; Wang, J.J. Synthesis and Fluorescence Sensing for  $Fe^{3+}$  and p-Nitrophenol of a Copper Coordination Polymer. *Chin. J. Inorg. Chem.* **2022**, *38*, 2539–2549.
16. Zeng, K.; Lei, L.; Wu, C.; Wu, K.B. Cobalt-based conjugated coordination polymers with tunable dimensions for electrochemical sensing of p-nitrophenol. *Anal. Chim. Acta* **2023**, *1279*, 341772. [[CrossRef](#)] [[PubMed](#)]
17. Zhao, L.; Han, Y.; Guo, G.; Bai, H.; Wang, Z.; Jing, H.; Song, G.; Wang, Z.; Li, J. Application of three Ln(III)-coordination polymers in fields of luminescence, antibacteria and detection of  $Fe^{3+}$  and 4-nitrophenol. *J. Rare Earths* **2023**, *41*, 1392–1397. [[CrossRef](#)]
18. Jin, K.; Hu, J.S.; Lv, C.N.; Liu, J.; Li, S.Y.; Cheng, T.T.; Zhou, C.H.; He, Z.W.; Zhang, M.D. A N-tripodal Ligand Cu-Based Coordination Polymer with Good Catalytic Activity for the Reduction of 4-Nitrophenol. *Chin. J. Struct. Chem.* **2017**, *36*, 1361–1367.
19. Zhang, X.F.; Jin, A. Cobalt(II) coordination polymer based on a carboxyl- triazolyl-bifunctional ligand: Synthesis, characterization and catalytic reduction of 4-nitrophenol. *Inorg. Chem. Commun.* **2020**, *119*, 108075. [[CrossRef](#)]
20. Aghajani, S.; Mohammadikish, M. Sustainable Coordination Polymer-Based Catalyst and Its Application in the Nitroaromatic Hydrogenation under Mild Conditions. *Langmuir* **2022**, *38*, 8686–8695.
21. Aditya, T.; Pal, A.; Pal, T. Nitroarene reduction: A trusted model reaction to test nanoparticle catalysts. *Chem. Commun.* **2015**, *51*, 9410–9431. [[CrossRef](#)] [[PubMed](#)]
22. Lotsch, B.V.; Schnick, W. New Light on an Old Story: Formation of Melam during Thermal Condensation of Melamine. *Chem. A Eur. J.* **2007**, *13*, 4956–4968. [[CrossRef](#)] [[PubMed](#)]
23. Burrow, J.N.; Ciufo, R.A.; Smith, L.A.; Wang, Y.; Calabro, D.C.; Henkelman, G.; Mullins, C.B. Calcium Poly(Heptazine Imide): A Covalent Heptazine Framework for Selective  $CO_2$  Adsorption. *ACS Nano* **2022**, *16*, 5393–5403. [[CrossRef](#)] [[PubMed](#)]
24. Bradley, J.N.; Thomas, D.C.I.M. 765. Metallo-organic compounds containing metal–nitrogen bonds. Part I. Some dialkylamino-derivatives of titanium and zirconium. *J. Chem. Soc.* **1960**, 3857–3861. [[CrossRef](#)]
25. Gorin, D.J.; Sherry, B.D.; Toste, F.D. Ligand Effects in Homogeneous Au Catalysis. *Chem. Rev.* **2008**, *108*, 3351–3378. [[CrossRef](#)] [[PubMed](#)]
26. Terzyk, A.P.; Bieniek, A.; Bolibok, P.; Wiśniewski, M.; Ferrer, P.; da Silva, I.; Kowalczyk, P. Stability of coordination polymers in water: State of the art and towards a methodology for nonporous materials. *Adsorption* **2019**, *25*, 1–11. [[CrossRef](#)]
27. Das, T.K.; Das, N.C. Advances on catalytic reduction of 4-nitrophenol by nanostructured materials as benchmark reaction. *Int. Nano Lett.* **2022**, *12*, 223–242. [[CrossRef](#)]
28. Choi, S.; Jeong, Y.; Yu, J. Spontaneous hydrolysis of borohydride required before its catalytic activation by metal nanoparticles. *Catal. Commun.* **2016**, *84*, 80–84. [[CrossRef](#)]
29. Shi, Y.; Zhou, Y.; Lou, Y.; Chen, Z.; Xiong, H.; Zhu, Y. Homogeneity of Supported Single-Atom Active Sites Boosting the Selective Catalytic Transformations. *Adv. Sci.* **2022**, *9*, 2201520. [[CrossRef](#)]
30. Duque, J.S.; Blandón, J.S.; Riascos, H. Localized Plasmon resonance in metal nanoparticles using Mie theory. *J. Phys. Conf. Ser.* **2017**, *850*, 012017. [[CrossRef](#)]
31. Leipzig, B. Über stufenweise Reduktion des Nitrobenzols mit begrenztem Kathodenpotential. *Z. Für Elektrochem.* **1898**, *4*, 506–514. [[CrossRef](#)]

32. Begum, R.; Rehan, R.; Farooqi, Z.H.; Butt, Z.; Ashraf, S. Physical chemistry of catalytic reduction of nitroarenes using various nanocatalytic systems: Past, present, and future. *J. Nanoparticle Res.* **2016**, *18*, 231. [[CrossRef](#)]
33. Jin, H.; Li, P.; Cui, P.; Shi, J.; Zhou, W.; Yu, X.; Song, W.; Cao, C. Unprecedentedly high activity and selectivity for hydrogenation of nitroarenes with single atomic Co1-N3P1 sites. *Nat. Commun.* **2022**, *13*, 723. [[CrossRef](#)] [[PubMed](#)]

**Disclaimer/Publisher's Note:** The statements, opinions and data contained in all publications are solely those of the individual author(s) and contributor(s) and not of MDPI and/or the editor(s). MDPI and/or the editor(s) disclaim responsibility for any injury to people or property resulting from any ideas, methods, instructions or products referred to in the content.